A Neoproterozoic ice advance sequence, Sperry Wash, California

M.E.BUSFIELD* & D.P. LE HERON

Department of Earth Sciences, Royal Holloway, University of London, Egham TW20 0EX, UK

*Corresponding author (email: Marie.Busfield.2011@live.rhul.ac.uk)

ABSTRACT

The Kingston Peak Formation is an archetypal Cryogenian succession that outcrops across the Death Valley region of eastern California. Above pre-glacial strata (KP1), two distinct glacial phases have been recognised and are interpreted to be allied to the panglacial Sturtian (KP2-3) and Marinoan (KP4) icehouse events. The thickest and most extensive unit, KP3, forms the entire exposed section at Sperry Wash. At this locality, ice-distal turbidites are succeeded by ice-medial and in turn ice-proximal facies, comprising a spectrum of IRD-bearing turbidites, debrites and shales. These are overlain by ice-marginal grounding-line fan deposits interbedded with glacitectonically deformed heterolithics, supporting local advance to an ice-contact position. The succession records accumulation within a glacier-fed subaqueous shelf, wherein the clear progradational signature is driven by ice advance towards the south-east. Evolution of the subaqueous complex is five-fold, comprising: 1) Ice distal outwash, 2) Build-out of ice-medial depositional lobes, 3) Ice proximal deposition and increased calving, 4) Resumed ice-margin advance, and 5) Growth of ice-contact grounding line fan. This sequence is unique in the Death Valley region for recording the first evidence of advance to ice-marginal and ice-contact settings, thereby enabling the location of the glacier terminus to be documented for the first time.

INTRODUCTION

The Cryogenian period (c. 720–635 Ma) is characterised by two of the most extensive glaciations recorded in Earth's history, broadly correlated to an older Sturtian (ca. 717-662 Ma; Zhou et al., 2004; Bowring et al., 2007; Macdonald et al., 2010) and younger Marinoan (ca. 635 Ma; Condon et al., 2005; Hoffmann et al., 2004) icehouse. Glacial deposits are recognised on almost all modern continents at various latitudes, described as a 'pan-glacial' state (Hoffman, 2009). Their accumulation within low-latitude and low-altitude settings led to the development of the snowball Earth hypothesis (Hoffman et al., 1998). Under a 'hard' snowball, pan-global ice sheets cover the Earth's surface, facilitating shutdown of the hydrological cycle. However, this hypothesis is inconsistent with widespread evidence for highly dynamic ice sheets and open water conditions (e.g. Arnaud, 2012; Busfield & Le Heron, 2013, 2014; Fleming, 2014; Le Heron et al., 2011; 2013; 2014a, b). The data are more supportive of a 'soft' snowball state wherein mobile, wet-based ice sheets are subject to multiple advance-retreat cycles, and separated by expanses of ice-free open waters (e.g. Fairchild & Kennedy, 2007). In order to improve understanding of the severity of Cryogenian glaciation, the glaciodynamics of Cryogenian ice masses need to be better constrained, and thus a detailed understanding of the extent and mobility of these ice sheets is required.

In eastern California, outstanding outcrops of the Pahrump Group preserve both the Sturtian and Marinoan glacial record, within the Kingston Peak Formation (Prave, 1999; Macdonald et al., 2013). These rocks are exposed in a broadly NW-SE trending outcrop belt spanning the Panamint Range and southeastern Death Valley (**Fig. 1**; Noble, 1934; Hazzard, 1937; Hewett, 1940, 1956; Wright et al., 1974; Macdonald et al. 2013). In the former region, strata belonging to the Kingston Peak Formation have undergone up to amphibolite grade metamorphism (Petterson et al., 2011b), whilst in the latter the metamorphic overprint is minimal, resulting in the preservation of primary sedimentary structures. The type section, the Kingston Range, exposes 300-2400 m of heterolithic siliciclastics with evidence of a clear glacial influence on deposition, characterised by two periods of glacial advance, separated by significant ice meltback (Le Heron et al., 2014b). These cycles record alternating ice-proximal to ice-distal conditions, within an exclusively proglacial setting. This study examines a spectacular exposure of the upper Kingston Peak Formation at Sperry Wash (Fig. 1), which demonstrates a clear ice advance signature from ice-distal to ice-marginal environments, with evidence of local advance to an ice-contact position. These deposits therefore represent the most ice-proximal settings recorded in the Death Valley region, and enable the position of

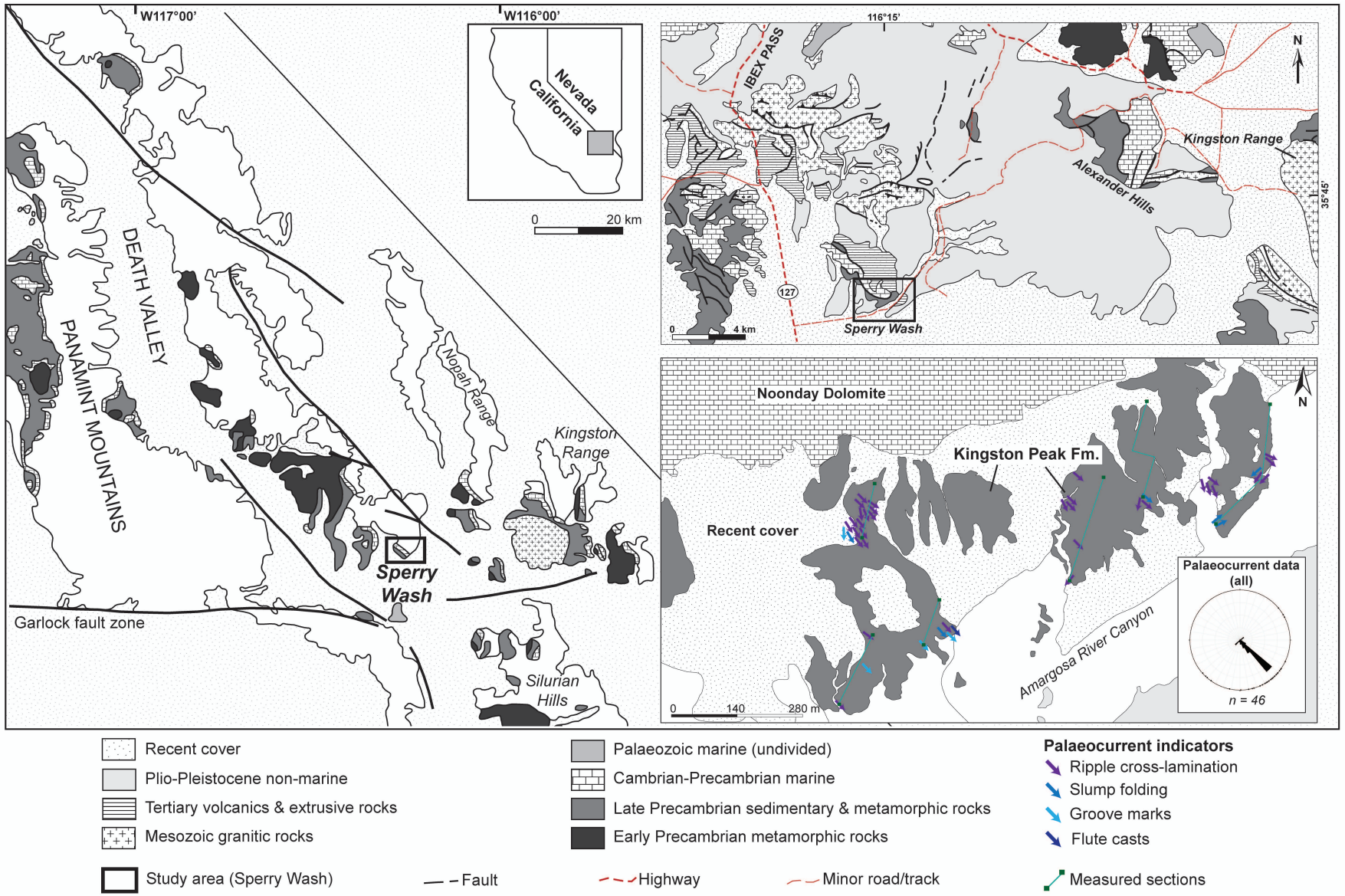

Fig. 1: A: NW-SE trending outcrop belt which exposes Pahrump Group strata throughout the Panamint Range and eastern Death Valley, modified from Macdonald et al. (2013). B: Geological map of south-eastern Death Valley region, including Sperry Wash study area, after Jennings et al. (1962). C: Map of study section demonstrating dip-corrected palaeoflow azimuths. Overall, a clear south-eastwards principle palaeoflow is recognised, with minor variability attributed to radial sediment distribution patterns and counter-flow slumping of unstable sediments (see text).

the tidewater terminus to be constrained for the first time.

GEOLOGICAL SETTING

The Kingston Peak Formation is the topmost member of the tripartite Pahrump Group, comprising the mixed carbonate and siliciclastic Crystal Spring Formation at its base, overlain by microbial carbonates of the Beck Spring Dolomite, and in turn the siliciclastic Kingston Peak. The lower Crystal Spring Formation is intruded by doleritesills dated at 1087 ± 3 Ma and 1067 ± 3 Ma (U-Pb baddeleyite ages, Heaman & Grotzinger, 1992), whilst detrital zircon ages place the upper member of the Crystal Spring Formation at younger than 787 ± 11 Ma (assigned to the Horse Thief Springs Formation, Mahon et al., 2014). The top of the Pahrump Group is truncated by an angular unconformity beneath the Ediacaran Noonday Dolomite (Prave, 1999; Petterson et al., 2011a), which is therefore used to argue for a minimum depositional age of 635 Ma (Hoffmann et al., 2004; Condon et al., 2005; Macdonald et al., 2013).

Deposition of the Pahrump Group spans both assembly and break-up of the Rodinian supercontinent along the southwestern margin of Laurentia (e.g. Mahon et al., 2014). The Kingston Peak Formation accumulated during early stages of intracratonic rifting, with evidence of syn-depositional tectonism in the form of buried normal faults and significant along-strike thickness changes throughout the Death Valley region, as well as extension-related volcanism in the Panamint Range (Troxel, 1966; Labotka et al., 1980; Hammond, 1983; Miller, 1985). Prave (1999) argues in favour of two discrete episodes of extension, broadly correlative with the older ('Sturtian') and younger ('Marinoan') glacial intervals, and cessation of rifting by the Ediacaran (i.e. deposition of the Noonday Dolomite).

In southeastern Death Valley, a four-fold stratigraphic subdivision (KP1-4) is commonly applied to the Kingston Peak Formation (Prave, 1999; Macdonald et al., 2013; Le Heron et al., 2014b). The basal KP1 is widely recognised as a pre-glacial succession (e.g. Prave, 1999), wherein its gradational basal contact supports inclusion in the previous (Beck Spring Dolomite) depositional cycle, and is argued to be genetically unrelated to the Kingston Peak Formation (Macdonald et al., 2013). In places, this unit is unconformably overlain by the laterally discontinuous Virgin Spring Limestone, which is in turn truncated by the overlying KP2. Units KP2 and KP3 are volumetrically the most abundant strata in southeastern Death Valley (Le Heron et al., 2014b), succeeded in places by thin, laterally impersistent exposures of KP4 (Macdonald et al., 2013). Based upon bounding unconformities, and correlation with strata in the Panamint Range, KP2 and KP3 are commonly attributed to the

older Cryogenian ('Sturtian') glaciation, and unit KP4 to the younger Cryogenian ('Marinoan') glaciation (Petterson et al. 2011b; Macdonald et al., 2013), and likewise to the earlier and later extensional regimes of Prave (1999).

This study will focus on an extremely well exposed section at Sperry Wash, southeastern Death Valley, which has not been subject to detailed sedimentological analysis in 50 years (supplemented in Troxel, 1982). The section is considered to correlate with member KP3 within the regional stratigraphic subdivision, although its stratigraphic thickness far exceeds correlative sections in the neighbouring Kingston Range (Le Heron et al., 2014b; Le Heron & Busfield, this volume). The greater preserved thickness permits development of a high resolution depositional history, which in tandem with the clear progradation from ice distal to ice-contact settings offers insight into a considerably more diverse spectrum of glacial depositional environments than recorded elsewhere in the Death Valley region.

FACIES ANALYSIS

The Sperry Wash succession crops out at the northern margin of the Armagosa river canyon, approximately 6 km from Interstate 127 (Death Valley Road) (**Fig. 1B,C**). At 200-300 m above sea level, the succession crops out in a hyper-arid basin and hence vegetation and soil-free outcrop conditions permit the collection of a high quality dataset. We measured a 636 m thick succession (**Fig. 2**), supplemented by a substantive palaeocurrent dataset (**Fig. 1C**). The base of the section is not exposed, whilst the top is truncated by an angular unconformity with the Noonday Dolomite which oversteps unit KP3 to the north and east (**Fig. 1C**). Five facies associations are recognised, and described below, including 1) Interbedded heterolithics, 2) Pebble to boulder conglomerate, 3) Diamictite, 4) Lonestone-bearing, and 5) Tectonised.

Interbedded heterolithics facies association

Description

This facies association comprises a heterogeneous assortment of stratified siltstone, sandstone and pebbly sandstone, and volumetrically is the most dominant facies in the studied section (**Fig. 2**). Deposits most frequently fine upwards (**Fig. 3A-B**), from massive coarse to pebbly sandstones into fine-grained sandstones, which infrequently preserve planar lamination. Both planar and irregular bed bases are recognised, whilst bed tops are planar throughout. Sandstone beds are separated by ungraded siltstones, which are predominantly parallel to ripple cross-laminated, though in some cases structureless. Thicker, uninterrupted

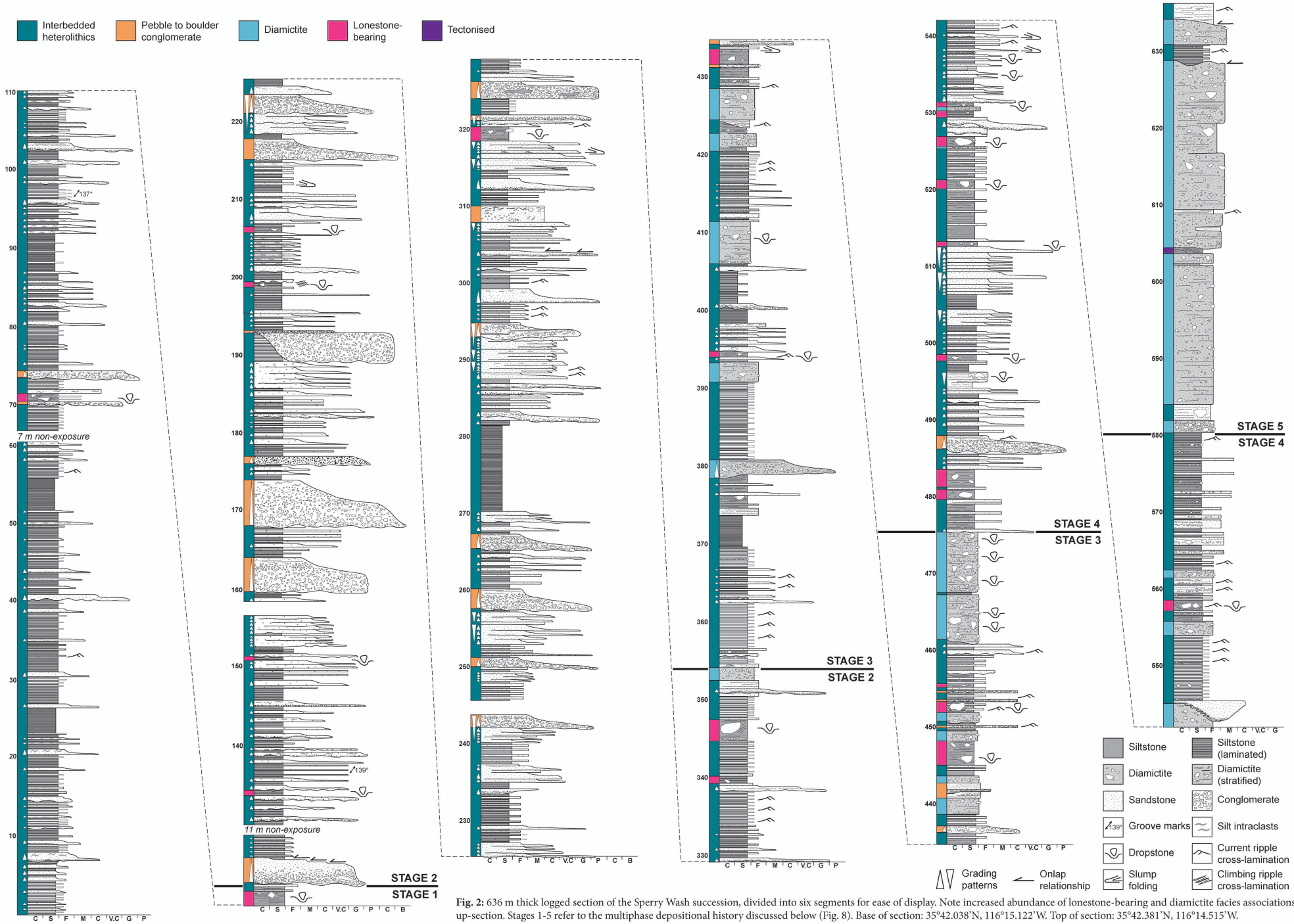

Fig. 2: 636 m thick logged section of the Sperry Wash succession, divided into six segments for ease of display. Note increased abundance of lonestone-bearing and diamictite facies associations up-section. Stages 1-5 refer to the multiphase depositional history discussed below (Fig. 8). Base of section: 35°42.038'N, 116°15.122'W. Top of section: 35°42.381'N, 116°14.515'W.

siltstone intervals are more common towards the base of the studied section (**Fig. 2**). As the proportion of sandstone increases upsection, more frequent and thicker sandstone interbeds occur, accumulating in places as amalgamated bedsets. These bedsets often preserve progressively thicker and coarser normally graded deposits, stacked in coarsening-upwards cycles (e.g. c. 220 m, c. 240 m, c. 290 m, **Fig. 2**), and commonly overlain by deposits of the pebble to boulder conglomerate facies association (**Fig. 3A-B**). Amalgamated sandstone beds infrequently show evidence of channelisation, characterised by erosive pebble-lined scours. An isolated erosively-based sandstone wedge is recorded at 545 m (**Figs. 2, 3C**), downcutting into the underlying diamictite facies association, where it exhibits a feather-edge, pebble lined contact. Towards the top of the studied section, ungraded sandstone interbeds dominate (above c. 340m, **Fig. 2**). These deposits are associated with intra-bed, bed parallel pebble horizons or clusters, in contrast to the normally-graded sediments where granule to pebble grade material is restricted to bed bases.

Within medium to coarse-grained sandstones, irregularly folded and convoluted siltstone intraclasts are common (**Fig. 3D**), particularly in the first 400 m of the logged section (**Fig. 2**). The intraclasts tend to occur near the top of sandstone beds. Rarely, sandstones also preserve recumbent and bed-parallel intrabed folds. Two examples of groove marks were observed at the sole of sandstone interbeds, trending 137° and 139° (c. 95 m and 146 m, **Fig. 2**; **Fig. 3E**). Current and climbing ripple cross-lamination within siltstones and fine-grained sandstones demonstrate foreset migration towards the south-east (**Fig. 3F**). Starved current ripple varieties (**Fig. 3G**) are typically associated with very finely laminated and delicately interbedded siltstone and fine sandstone, giving a 'banded' appearance to the strata (**Fig. 3H**). These sediments are also associated with bed-parallel pebble horizons or clusters.

Interpretation

The predominant normally-graded facies are interpreted to record a spectrum of high to low-density T_{ABC} turbidites, supported by the presence of groove marks and flute casts on the soles of some sandstone beds. The abundant massive sandstone component indicates deposition via high-density turbidity currents (T_A), where elevated near-bed sediment concentrations dampen turbulence and promote rapid deposition, and thus hinder bedform development (Kuenen, 1966; Middleton & Hampton, 1973; Talling et al. 2012). Planar-laminated intervals reflect deposition from high-density traction carpets (T_{B2} or T_{B3}; Talling et al. 2012), where sediment fallout rates drop sufficiently to enable lateral shearing near

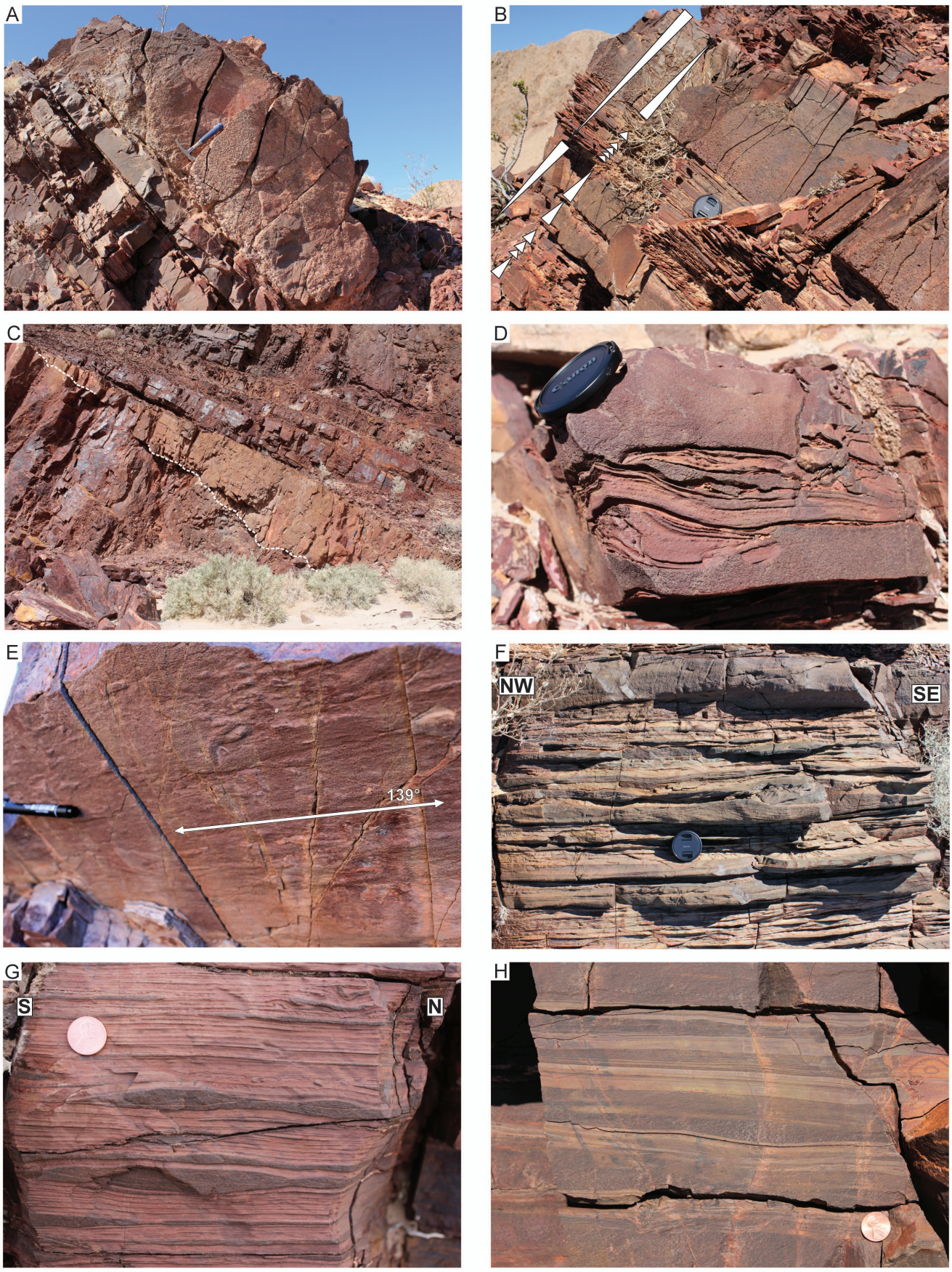

Fig. 3: Interbedded heterolithics facies association. Hammer: 26 cm, Lens Cap: 5 cm, Coin: 1.9 cm, Pen Tip, 0.9 cm. A-B) Thickening and coarsening-upwards normally graded bedsets, capped by pebble to boulder conglomerate facies association in A; C) White dashed line picks out pebble-lined channel feature at c. 543 m (Fig. 2); D) Irregular and convolute rip-up silt intraclast; E) Groove marks on base of sandstone bed trending 139°; F) Ripple cross-lamination, foreset migration towards south-east; G) Starved ripple foresets, frequently associated with H) Finely interbedded sandstone and siltstone, displaying striking 'banded' appearance.

the base of the flow (Lowe, 1988; Leclair & Arnott, 2005; Sumner et al., 2008). Such traction carpets are commonly found in association with high-density T_A facies (Talling et al. 2012). Irregular, convoluted silt intraclasts in the sandstone beds are interpreted as rip-up clasts, incorporated through erosion and 'plucking' of semi-lithified interbedded siltstone facies. They are likewise interpreted to reflect lower sediment fallout rates, thereby minimising their break-up during transport. Their organisation along discrete horizons towards bed tops provides further credence to their transport within turbidity currents, as opposed to debris flows which would deposit chaotically distributed mud clasts (Talling et al., 2012).

Distinct coarsening-upward packages composed of normally-graded sandstone beds are interpreted as depositional lobe elements (Prélat et al., 2009; Macdonald et al., 2011). In the stratigraphic hierarchy of Prélat et al. (2009), lobe elements are built up from individual beds and bedsets, and stack to form lobes, which in turn build up to form a lobe complex. The high sand to mud ratio and common bed amalgamation within these packages supports an axis to off-axis position within the lobe complex (Prélat et al., 2009; Prélat & Hodgson, 2013). Such thickening and coarsening-upward trends are commonly recognised within depositional lobes (e.g. Hodgson et al., 2006; Prélat et al., 2009; Macdonald et al., 2011 and references within). This behaviour demonstrates initiation and growth of the lobe/lobe elements towards a fixed point, which could be basinward or across strike and therefore is not exclusively diagnostic of progradation (Prélat & Hodgson, 2013).

Ripple cross-laminated sandstone and siltstone units reflect fully turbulent near-bed conditions within low-density turbidity currents (T_C; Mulder & Alexander, 2001; Baas et al., 2011; Talling et al., 2012), where turbulence is no longer dampened under much lower sediment fallout rates (e.g. Walker, 1967, 1978; Piper, 1978; Allen, 1982; Komar, 1985; Sylvester & Lowe, 2004). These ripples become 'starved' under elevated rates of tractional re-working (Talling et al., 2007; Talling et al., 2012). Climbing ripple cross-lamination is also indicative of fully turbulent flow conditions, but under more rapid rates of sediment delivery (Kuenen & Humbert, 1969; Allen, 1991; Baas, 2000; Kane & Hodgson, 2010; Jobe et al., 2012). Rare recumbent intrabed folds also support high rates of sediment delivery to induce instability and slumping (e.g. Maltman, 1994). Ripple cross-laminated intervals are commonly bounded by laminated and less frequently massive siltstone horizons, interpreted as densite mud deposited via a combination of low-density turbidity currents (T_D or T_{E-1}; Talling et al. 2012) and hemipelagic fallout during waning flow (e.g. Allen et al., 2004). Both T_D and T_{E-1} intervals are characteristically very thin (e.g. Walker,

1967, 1978; Piper, 1978; Allen, 1982; Komar, 1985; Sylvester & Lowe, 2004; Talling et al., 2012), and hence waning flow processes are favoured here. These sediments are thought to accumulate on the fringe and distal fringe of the lobe complex (Prélat et al., 2009). Irregular basal contacts of sandstone interbeds record erosion and cannibalisation during repeated emplacement of subaqueous flows. The isolated, erosively-based sandstone wedge is interpreted as a channel fill, the origin of which will be discussed below. Planar, non-erosive basal contacts are interpreted as the product of hydroplaning at the head of the flow (e.g. Laberg & Vorren, 2000), and 'shear wetting' within the body of the flow (e.g. Ilstad et al., 2004), both of which act to lubricate the base of the flow and protect underlying beds from cannibalisation (Talling, 2013). As such, this switch to non-erosive behaviour is likely driven by elevated water contents, within more dilute flows, which would facilitate basal lubrication.

Pebble to boulder conglomerate facies association

Description

This facies association outcrops intermittently throughout the basal two thirds of the studied section, with the first recorded appearance at c. 70 m (**Fig. 2**). Deposits are predominantly massive, highly-concentrated conglomerates with both clast- and matrix-supported textures. Basal contacts are irregular, downcutting sediments of the interbedded heterolithics facies association (**Fig. 4A**), whilst upper contacts with these facies are sharp and planar. Channel-like geometries are frequently observed (**Fig. 4B**). The conglomerates commonly fine upwards from cobble-pebble grades, through coarse to medium-grained sandstones (**Fig. 4A,C**). Crude stratification occurs in the sandier intervals. Other beds appear to be ungraded, fining upwards only at the very top. Clasts include karstified carbonate from the Beck Spring Dolomite and Crystal Spring Formation, with subordinate quartzite. They are predominantly sub-angular, though rounded clasts are also present. As seen in the interbedded heterolithics facies association, irregularly folded and convoluted siltstone intraclasts are preserved towards the top of fining-upward units, within the clast-poor sandier intervals. Isolated examples of sand-grade intraclasts are also recorded within one normally-graded conglomerate unit (c. 115 m, **Fig. 2**).

Interpretation

Representing the product of hyperconcentrated sediment gravity flows (Lowe, 1982; Kneller, 1995; Mulder & Alexander, 2001; Winsemann et al., 2007; Talling et al., 2012), the pebble to boulder conglomerates are high-density

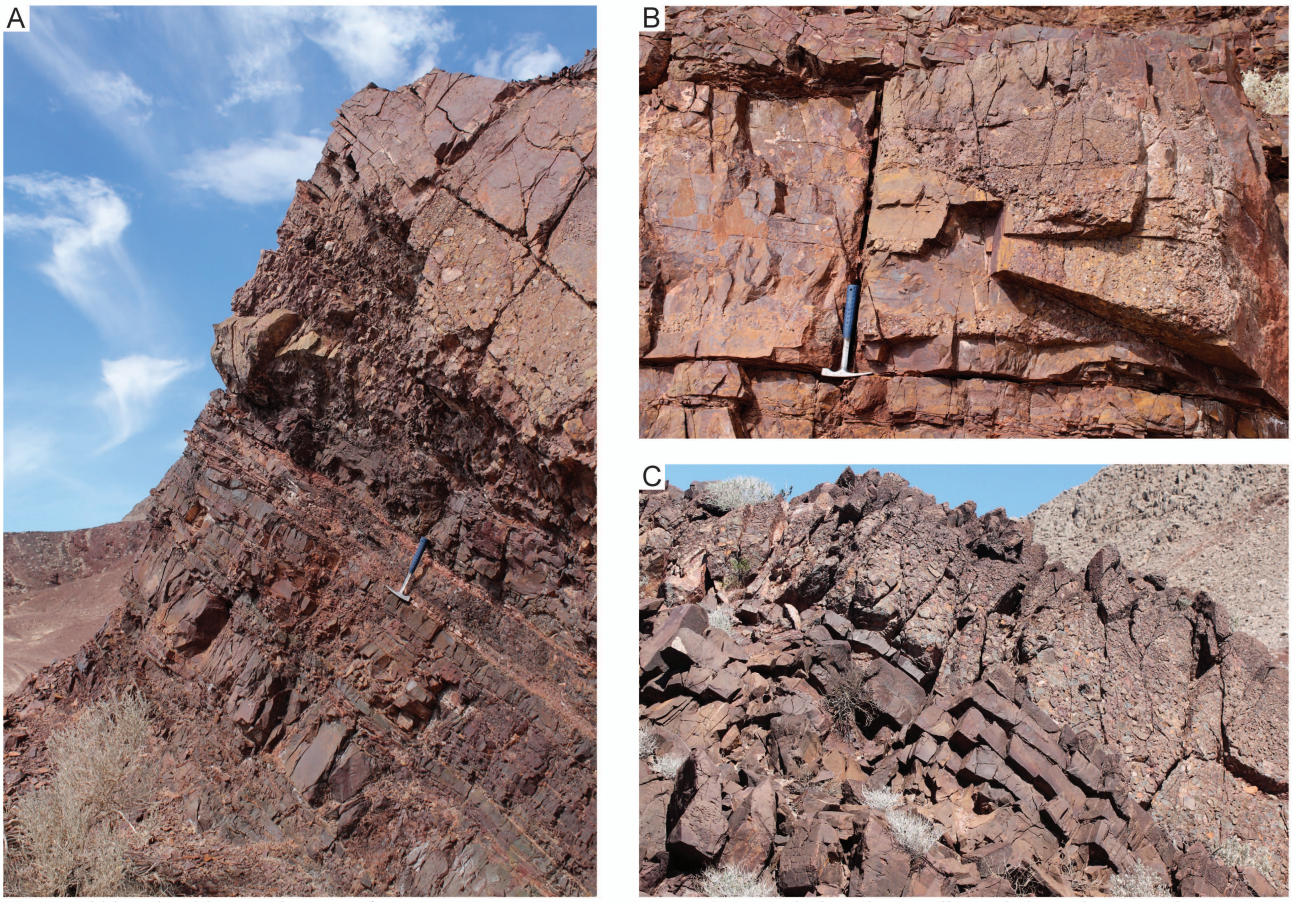

Fig. 4: Pebble to boulder conglomerate facies association. Hammer: 26 cm. A) Erosively-based normally graded conglomerate downcutting the interbedded heterolithics facies association; B) Internal channelization within normally-graded conglomerate faciea; C) Conglomerate demarcates top of coarsening and thickening-upwards bedsets.

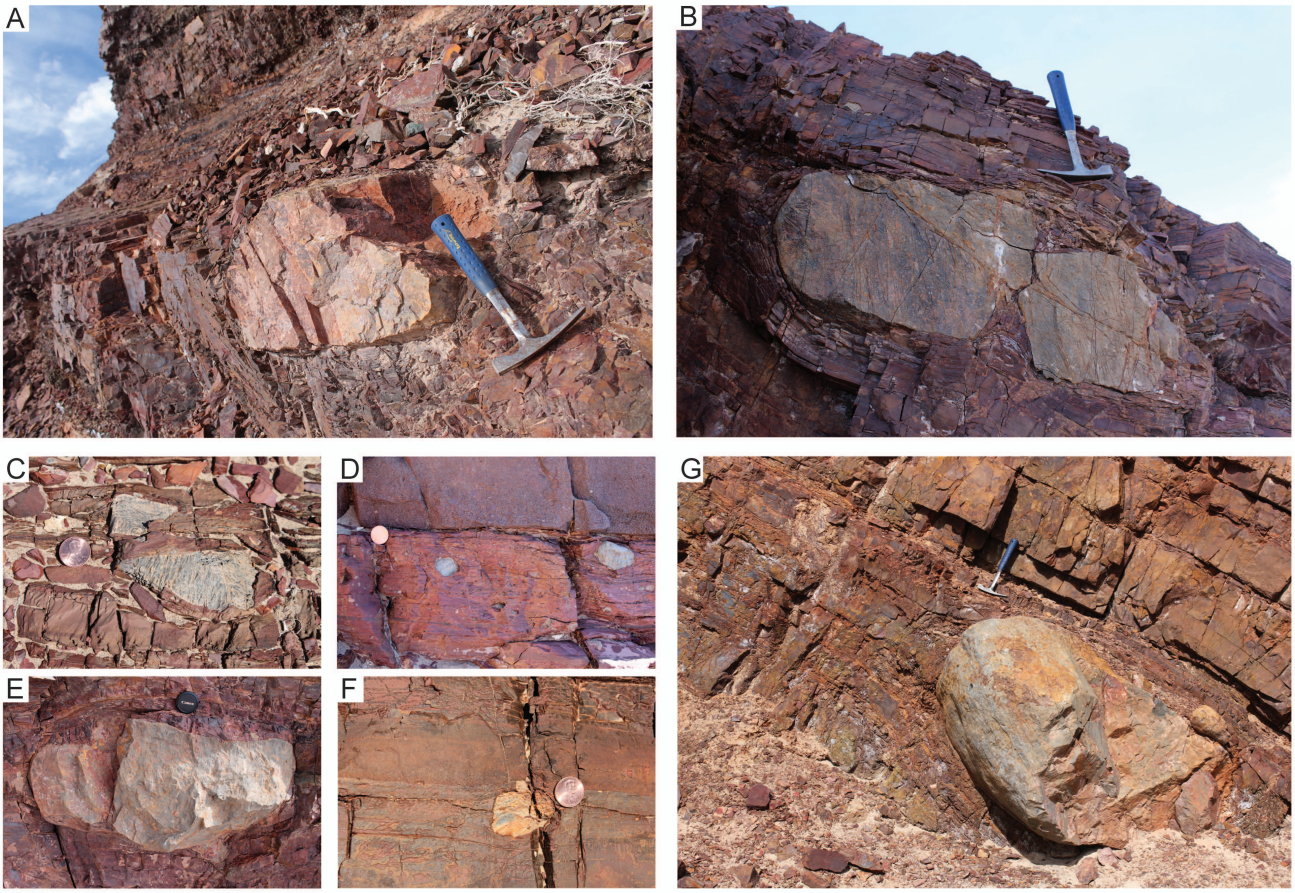

Fig. 5: Lonestone-bearing facies association. Hammer: 26 cm, Lens Cap: 5 cm, Coin: 1.9 cm. A-G) Small pebble to large boulder sized lonestones with impact-related deformation structures, within both crudely and well laminated siltstone and sandstone facies.

equivalents of the interbedded heterolithics facies association. Higher sediment concentrations are indicated by commonly erosive basal contacts and general absence of sedimentary structures. The latter is the result of hindered settling from high-density flows, typically characterised by rapid deposition and dampened turbulence (Talling et al., 2012). Beds which are predominantly ungraded are interpreted as moderate cohesive strength debris flows, where matrix mud content is too low to be fully cohesive, and too high for non-cohesive flows (*sensu* Talling et al., 2012). Moreover, moderate cohesive strength flows are more susceptible to flow transformation, generating normally-graded upper contacts where the flow mixes with the overlying water column. The predominant normally-graded conglomerate beds are thus considered to reflect co-genetic high-density turbidites, derived through further dilution and mixing during downslope movement (Hampton, 1972; Talling et al., 2012). The preservation of siltstone intraclasts towards the top of conglomerate beds must therefore reflect more dilute, low-density flow conditions, where lower sediment fallout rates inhibit disaggregation of the intraclasts.

The conglomerate beds commonly occur at the top of coarsening-upward packages of the interbedded heterolithics facies association, and thus represent the topmost lobe element within the lobe (sensu Prélat et al., 2009). Their coarse calibre likely indicates a lobe axis position, and may correlate with the period of maximum lobe building prior to lobe switching or abandonment. This is supported by the consistent occurrence of fringe/distal fringe silt facies above the conglomerate beds.

Lonestone-bearing facies association

Description

This facies association occurs in thin (<5 m), comparatively rare horizons throughout the studied section, albeit with greater abundance above 430 m (**Fig. 2**). Well stratified parallel-laminated siltstones, and rare interbedded sandstones, are characteristic. The siltstones locally show current and climbing ripple-cross lamination. Normal grading, a classic feature of the heterolithic facies association, is not recorded (**Fig. 2**). Moreover, outsized clasts do not occur as bed-parallel clast trains or clusters, but as isolated lonestones, frequently puncturing and downwarping underlying laminae, and in turn draped by overlying laminae (**Fig. 5A-G**). Outsized clasts range from pebble to large boulder (up to 1 m) in size, and consist predominantly of Beck Spring Dolomite, in tandem with the pebble to boulder conglomerate and diamictite facies associations.

Interpretation

These deposits are considered to accumulate via dilute, low-density turbidity currents and settling of hemipelagic fines during waning flow conditions. The facies are closely associated with normally-graded turbidites of the interbedded heterolithics facies association, lending support to their co-genetic subaqueous density flow origin. Evidence of current and climbing ripple cross-lamination indicates fully turbulent conditions within low-density turbidity currents (T_C; Mulder & Alexander, 2001; Baas et al., 2011; Talling et al., 2012). The predominance of parallel lamination may be associated either with waning low-density turbidity currents (T_D or T_{E-1}; Talling et al., 2012), or hemipelagic fallout during quiescent phases (e.g. Allen et al., 2004). Abundant outsized clasts with impact structures within these finely laminated turbidites are interpreted as ice-rafted debris (IRD). The low-density subaqueous flows and preservation of delicate ripple structures preclude sediment flow rafting of the outsized clast fraction (e.g. Postma et al., 1988).

Diamictite facies association

Description

These deposits are first recorded at 343 m, and become progressively more abundant upwards, accumulating as up to 20 m thick units at the top of the logged section (**Fig. 2**). They are readily differentiated from the pebble to boulder conglomerate facies association by their poor sorting, especially visible in the diverse spectrum of granule to large boulder sized clasts within individual beds, and typically higher matrix content. The facies are predominantly ungraded, although an isolated normally-graded bed is recorded at 380 m. Upper and lower bed contacts are commonly planar and conformable; erosive basal contacts, downcutting facies of the underlying interbedded heterolithics facies association, are rarely recorded. In places, the upper contacts of diamictite beds are highly irregular, where they are typically onlapped by siltstones and sandstones of the interbedded heterolithics facies association (**Fig. 2**).

Diamictite facies include both massive and stratified varieties, with crudely stratified units dominant. Clasts range from small pebble to boulder, and consist of Beck Spring Dolomite and Crystal Spring Formation carbonates, with occasional quartzite clasts (**Fig. 6A-F**). In contrast to the pebble to boulder conglomerate facies association, clasts are predominantly rounded to well-rounded, with infrequent sub-angular morphologies. Isolated beds <5 m thick, are typical (**Fig. 2**). However, thicker beds occur between 460-475 where they contain abundant cobble to boulder-sized clasts (**Fig. 6A-F**), some of which are striated (**Fig. 6G**), and

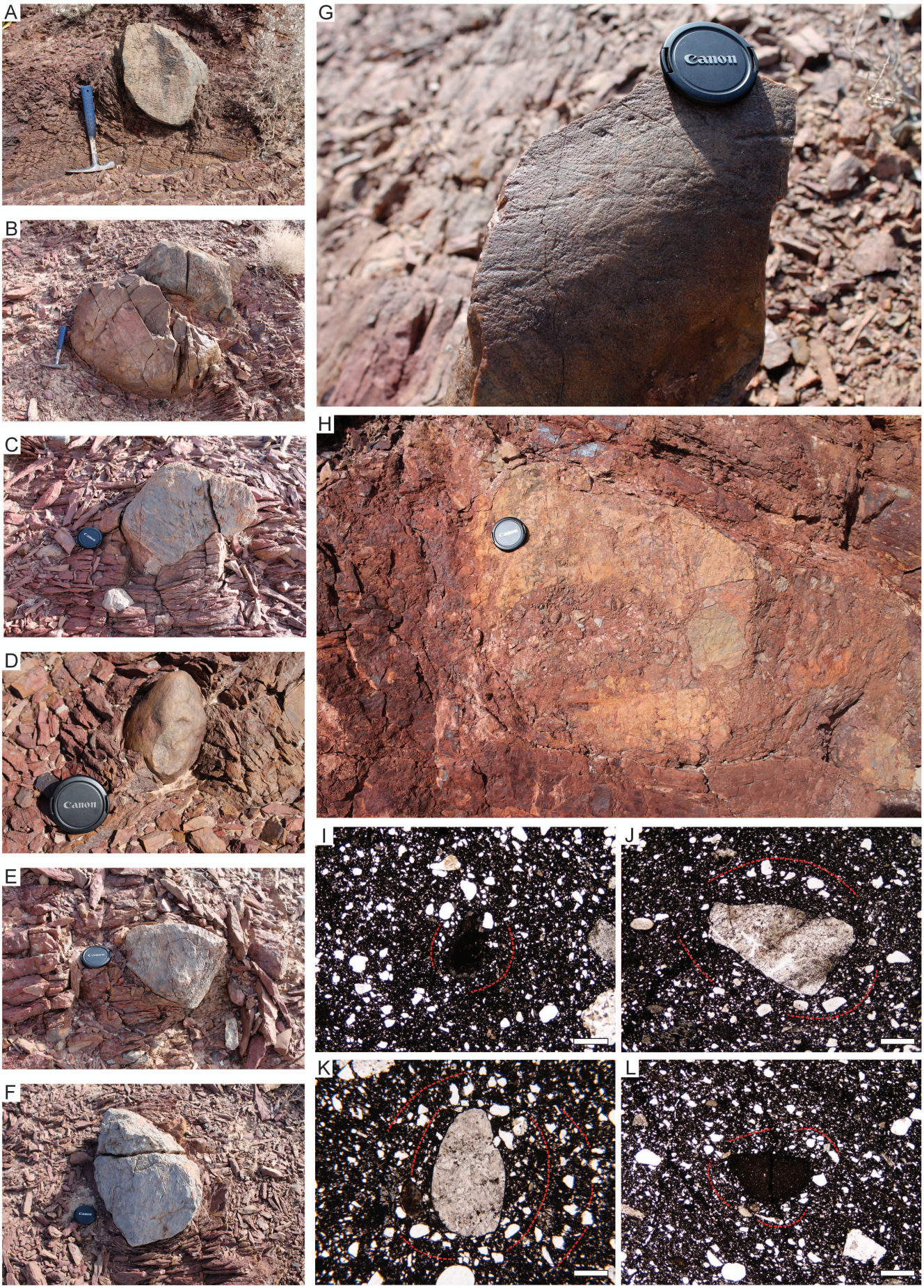

Fig. 6: Diamictite facies association. Hammer, 26 cm, Lens Cap: 5 cm. A-F) High concentration of outsized clasts with impact-related deformation structures (460-475 m, Fig. 2); G) Striated clast associated with IRD-rich diamictite unit (460-475 m, Fig. 2); H) Fragmented carbonate clast, cavity infilled by surrounding diamictite. Jig-saw fit fragments support in situ fracturing; I-L) Bar width = 1 mm. Examples of arcuate grain alignments: smaller grains demonstrate circular arrangement around larger 'core stone'.

the majority of which downwarp and puncture underlying laminae. Towards the top of the logged section (above 560 m: **Fig. 2**), downwarping relationships beneath the outsized clasts disappear.

Thick, almost continuous packages of diamictite (up to 20 m thick) return around 584 m, where they are locally interbedded with <1 m thick units of laminated siltstones and sandstones. These diamictite packages, whilst still matrix-supported, are notably clast-rich compared to underlying diamcitite facies, with a higher proportion of coarser pebble, cobble and boulder sized clasts. At 604 m the sequence is interrupted by a thin deposit of the of the tectonised facies association. Diamictite immediately overlying this interval exhibits small-scale folds verging south-east, in addition to a fragmented carbonate boulder, where the interstitial space is infilled with the matrix-rich diamictite of the host sediment (**Fig. 6H**). On the micro-scale, the surrounding diamictite exhibits arcuate grain alignments, wherein grains are arranged in a circular pattern around a core stone, or area of more rigid matrix (**Fig. 6I-L**).

Interpretation

With the exception of the thick diamictite packages, at 460-475 m and >584 m, this facies association consistently occurs as isolated, thin beds bounded by subaqueous density flow deposits of the interbedded heterolithics and lonestone-bearing facies associations. The absence of grading and pervasive crude stratification is typical of gravitationally re-worked diamictites (e.g. Evans & Pudsey, 2002; Powell & Domack, 2002; Marenssi et al., 2005; Henry et al., 2012), commonly encountered within glacial regimes due to the rapid, dynamic and waterlain mode of sediment delivery, and resultant instability of the sediment pile (Elverhøi et al., 2002; Ó'Cofaigh et al., 2002; Powell & Domack, 2002). Their repeated stratigraphic association with the s and lonestone-bearing turbidite facies is used to support flow transformation, and generation of 'linked' turbidity currents. This process occurs through flow dilution during sediment re-working by mixing with the overlying water column, and is more effective on moderate cohesive strength debris flows, as higher cohesive strengths hinder mixing (Mulder & Alexander, 2001; Talling et al., 2012). Flow transformation is further corroborated by the occurrence of a normally-graded diamictite bed at 380 m, interpreted to reflect more dilute, turbulent flow conditions towards the top of the bed. Outsized clasts which downwarp and puncture underlying laminae are interpreted as iceberg rafted debris (IRD). Their relative rarity within the isolated, thin diamictite beds characteristic of the lower succession is attributed to the combined influence of re-working during density flow remobilisation, and less proximal position to the ice front, discussed below.

Within the first pronounced thickness of diamictite, at 460-475 m, a noteworthy increase in abundance of IRD is evident, alongside the first appearance of striated clasts in the logged section. The latter, indicative of subglacial debris entrainment (Boulton, 1978), were notably absent from the gravitationally re-worked diamictite facies, where clast-on-clast abrasion is anticipated to remove striations during remobilisation (Le Heron et al., 2013, 2014b). Their preservation, in tandem with abundant IRD is used to support deposition within an iceberg rain-out deposit, wherein striated clast varieties could be transported basinward within icebergs without significant abrasion. The considerable increase in abundance of IRD is considered to reflect greater instability at the ice front, driving enhanced calving processes and iceberg distribution. Well preserved impact structures beneath these dropstones are suggestive of minimal re-working, thus representing the product of highly concentrated, *in situ* rain-out. It is anticipated that icebergs would lose considerable debris during transport away from the ice front, particularly the coarser debris load, and therefore such an abundance of cobble to boulder grade IRD is more typical of ice-proximal settings. The introduction of subglacially striated boulders into the clast assemblage at this interval is also considered to corroborate a more proximal terminus position.

The second thick accumulation of this facies association (>584 m) records thicker, uninterrupted units of diamictite with an abundance of pebble, cobble and boulder sized clasts, but a complete absence of impact-related deformation structures. This is interpreted to reflect more voluminous and rapid rates of sediment supply, promoting elevated and sustained ice-rafting processes into a thick and inherently unstable sediment pile, wherein delicate impact structures could be readily overprinted. This scenario is typical of debris-laden, ice-marginal settings where high volumes of coarse, poorly sorted debris flows commonly accumulate as grounding-line fans. In the ancient record, these systems are commonly devoid of impact-related deformation structures (e.g. Lønne, 1995), despite evidence supporting active ice-rafting within comparable modern ice front environments (Ovenshine, 1970; Dowdeswell, 1986, 1989). This may be due in part to (1) the lithological and textural similarity between the rafted material and the 'host' fan deposits (cf. Lønne, 1995), (2) sediment remobilisation driven by periodically unstable fan-slope collapses, or (3) current re-working through subglacial meltwater discharge. The latter process may also contribute to the development of crude stratification within the diamictite facies at this interval through minor re-working and removal of fines. It is proposed these fine grained sediments are remobilised as dilute, low-density turbidity currents and deposited in ephemeral channels on the grounding-line

fan, thereby accumulating locally as interbedded siltstones and sandstones.

Both the small-scale folds verging towards the SE and the fragmented carbonate clast are interpreted as syn-sedimentary deformation features. The recorded fold vergence parallels principal palaeoflow orientations recorded throughout the succession (**Fig. 1C**), whilst the 'jig-saw fit' pattern of the clast fragments, and infill of the interstitial space by the surrounding diamictite matrix, suggests *in situ* fracturing under soft sediment conditions. Within an ice-marginal fan system, these processes could be driven by either sediment remobilisation or glacitectonic deformation, wherein both have the capacity to produce a similar suite of deformation structures. For example, the micro-scale arcuate grain alignments are a common feature of both subglacial environments and sediment density flows (Lachniet et al., 2001; Menzies & Zaniewski, 2003; Phillips, 2006). Whilst in both scenarios, clast fracturing can be driven by pronounced pressure gradients within the deforming bed, varying from the highest strain conditions at the base of sediment gravity flows due to contact with the underlying substrate, or towards the top of glacitectonic sequences near the ice-bed interface. The significance of these features will be discussed in the context of the immediately underlying tectonised facies below.

Tectonised facies association

Description

This facies association is restricted to a single, c. 1 m thick horizon at 604 m (**Fig. 2**). It consists of finely interbedded fine-grained sandstones and siltstones that bear granule to small pebble sized clasts. These well-stratified sediments are deformed into a series of south-east verging folds which ramp up relative to bedding (**Fig. 7A**). Stratified sediments within the fold limb also show small (<1 cm), local offsets. Note that deformation is entirely confined to this facies association, neither affecting underlying nor overlying strata of the diamictite facies association.

On the micro-
horizons are normally graded, with clear load structures at their bases (**Fig. 7B**). Outsized clasts appear to 'sink' into their host siltstone or sandstone laminae, although evidence of clear downwarping or puncturing of laminae is absent. Laminae are locally displaced by minor fault offsets and deformed into open folds verging towards the south-east. In places, intraclasts of the finely interbedded siltstone and sandstone laminae occur as angular, randomly oriented fragments. The more clay-rich intervals display weak to moderate birefringence, either as linear zones of more birefringent clay minerals, or as zones of elevated birefringence with no clear preferred orientation, characterised in micromorphological

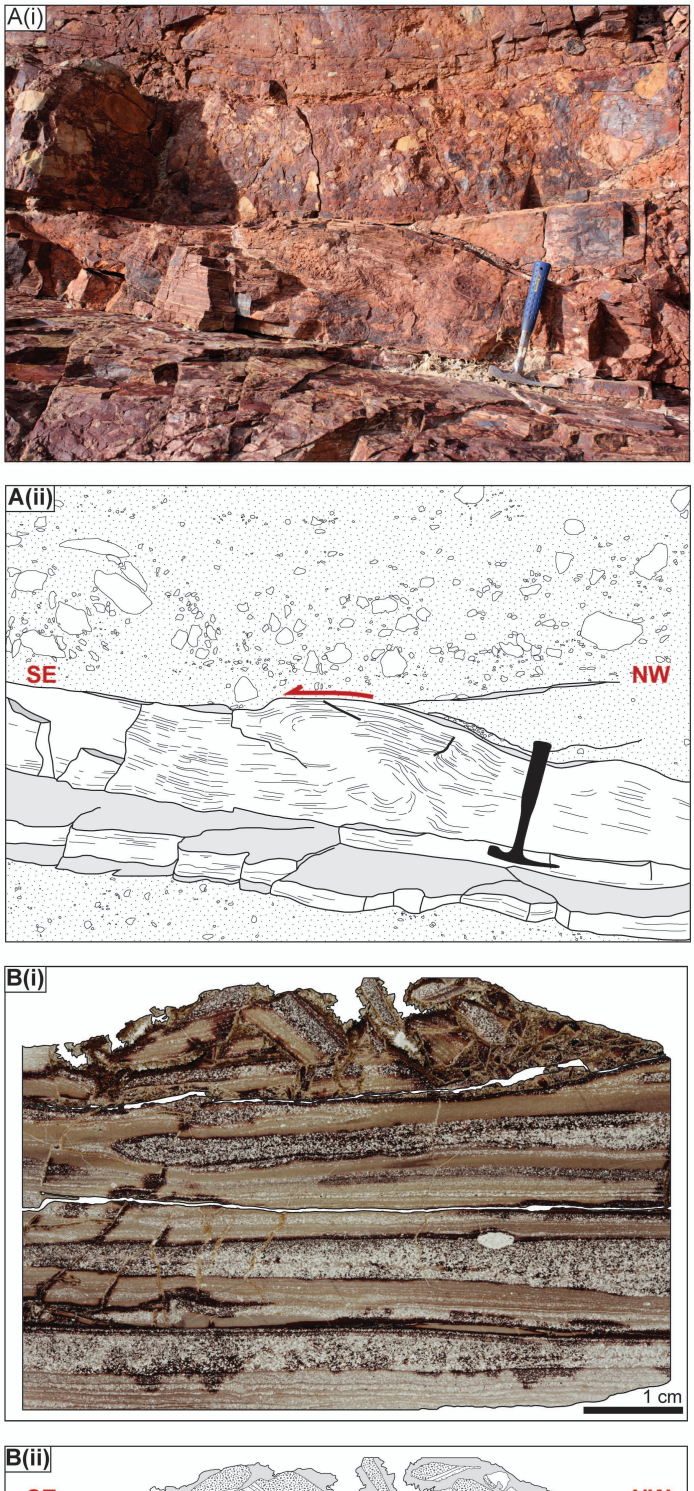

Fig. 7: Tectonised facies association. Hammer: 26 cm. A(i-ii) Macro-scale photo and interpretive overlay of fold structures verging and ramping up towards the south-east. Note small fault offsets within limb of fold structure. B(i-ii) Micro-scale photo and interpretive overlay shows well-laminated normally-graded sediments, in places deformed into south-east verging folds. Clasts appear to sink into underlying laminae, although unclear whether ice-rafted. Top of section shows randomly oriented fragments of laminated sediment, reflecting brittle deformation and re-organisation.

terms as unistrial and asepic plasmic fabrics, respectively (for definitions see Zaniewski & van der Meer, 2005).

Interpretation

As with the lonestone-bearing facies association, these sediments record deposition by low-density turbidity currents and background hemipelagic sedimentation. Their close stratigraphic relationship with the diamictite facies association suggests these fine grained sediments may have been winnowed and deposited in ephemeral channels on the grounding-line fan, in a similar manner to the interbedded siltstones and sandstones of the diamictite facies association discussed above. In contrast to these sediments, dilute turbidites within the tectonised facies association are then deformed into a series of SE-verging folds.

Within ancient successions, discriminating between sedimentary and tectonic origins for deformed strata is crucial. In this case, deformation is clearly restricted to one horizon, and does not affect underlying sediments, with only minimal deformation in the immediately overlying diamictite. Moreover, deformation is not facies dependent, and thus equivalent facies elsewhere in the succession (low-density turbidites of the lonestone-bearing facies association and diamictite facies association) are also undeformed (e.g. Fleming, 2014). Finally, the succession as a whole demonstrates no pervasive deformation or cleavage development, in contrast to correlative sections in the Panamint Range (Petterson et al., 2011b). The dominant ductile style of folding is therefore considered indicative of soft sediment deformation, potentially facilitated by elevated water contents as would be typical of dilute, low-density flows. Given the proximity of the ice margin, it is recognised that meltwater input could also contribute significantly to these higher porewater pressures. During deformation, elevated fluid contents can become overpressurised, promoting rapid water expulsion concomitant with a switch to more brittle styles of deformation (e.g. Denis et al., 2010; Ravier et al., 2014). This process is interpreted to account for the small fault offsets observed displacing the limbs of the fold structures, in addition to the fracturing and angular fragmentation of the sediments on the micro-scale.

In ice-marginal settings, soft sediment deformation could be the product of either sediment remobilisation or glacitectonic deformation, wherein both proglacial and subglacial processes are plausible. Sediment instability and failure frequently occur due to rapid and high rates of sediment supply. Deposits of the tectonised facies association, accumulating within ephemeral channels on the grounding-line fan, could therefore have undergone either slump-related deformation driven by internal instability, or subsequently been deformed beneath an overriding coarse debris flow during fan

build-out. However, sediment gravity flow deformation observed throughout the remainder of the succession, particularly within the interbedded heterolithics facies association, generates consistently recumbent and bed-parallel folds. In contrast, within the tectonised facies association, fold structures ramp upwards, where folds essentially 'piggy-back' underlying fold structures towards the south-east (**Fig. 7A**). Arguably, the deposits could have been deformed through a bulldozing motion at the head of an advancing debris flow, but it is perhaps surprising that they were not then eroded and cannibalised within the significantly coarser and more competent flow. Although it is recognised that such erosion could account for the limited preservation of this facies association. Overall, common features considered characteristic of sediment re-working in the tectonised facies association are curiously absent on both the macro-scale (clasts with diamictite coatings, load structures, vertical water escape structures) and micro-scale (flow noses, tile structures, laminated grain coatings) (see Busfield & Le Heron, 2013 and references within).

An alternative scenario, especially in light of the evidence favouring increasing proximity of the ice front throughout the succession (see discussion below), is that deformation occurs ahead of or beneath the advancing glacier terminus. In ice-contact settings, the elevated water contents argued to facilitate the dominantly ductile style of deformation would be further enhanced by input of both subglacial and englacial meltwater, as well as the high confining pressure of the overriding ice (Menzies, 2000; Phillips et al., 2007; Lee & Phillips, 2008; Busfield & Le Heron, 2013). This is supported by the presence of unistrial plasmic fabrics, reflecting development of high strain planar shear fabrics within the deforming bed (e.g. Hiemstra & Rijsdijk, 2003; Busfield & Le Heron, 2013). In this scenario, the ramping-upwards style of folding is considered to reflect ice-marginal deformation through glacitectonic thrusting (e.g. Ó'Cofaigh et al., 2011; Evans et al., 2012), rather than the widespread isoclinal folding typical of shearing within the subglacial bed (e.g. Lee & Phillips, 2008; Busfield & Le Heron, 2013). Glacitectonic thrusting alongside a high sediment supply frequently results in the development of thick sediment piles in ice-marginal settings (e.g. Evans & Hiemstra, 2005; O'Cofaigh et al., 2011; Evans et al., 2012), which could contribute to the notably thick accumulation of the diamictite facies association at the top of the logged section.

In light of the limited evidence of features diagnostic of sediment gravity flow deformation, the unique 'piggy-back' style of folding, the development of unistrial plasmic fabrics, typically associated with higher strain conditions than developed through mass flow processes, and the clear evidence for an

advancing ice margin throughout deposition of the Sperry Wash succession, proglacial glacitectonic deformation of the ice-marginal grounding-line fan is favoured here. However, it is contended that deformation of the tectonised facies association could plausibly have been driven by bulldozing at the head of a diamictic debris flow. In both situations, deformation is interpreted to occur immediately adjacent to the ice margin, where the advancing glacier terminus delivered extremely high volumes of coarse, poorly sorted debris (diamictite facies association), most likely contributing to localised ice-contact deformation of the grounding-line fan.

PALAEOCURRENT INDICATORS

Numerous palaeocurrent indicators are recorded throughout the Sperry Wash succession, predominantly within the interbedded heterolithics and lonestone-bearing facies associations (**Fig. 2**). These include ripple cross-lamination and soft sediment slump folding, as well as groove marks and flute casts on the base of turbidite beds. Dip corrected azimuths demonstrate principal palaeoflow towards the south-east at all stratigraphic levels (**Fig. 1C**). This is corroborated by the south-east verging glacitectonic fold structures within the tectonised facies association. These data therefore act to support south-eastwards palaeo-ice flow. Towards the top of the studied section, isolated examples of slump folds verging north-east (**Fig. 1C**) are interpreted to reflect collapse of an unstable sediment pile as opposed to a change in sediment provenance. Whilst limited evidence of palaeoflow towards the south/south-west likely reflects a degree of radial distribution within the subaqueous fan complex.

EVOLUTION OF A GLACIER-FED SUBAQUEOUS SYSTEM

The Sperry Wash section demonstrates a clear and pervasive glacial signature throughout, which significantly becomes more pronounced upsection. The predominance of subaqueous sediment gravity flow deposits is consistent with an active, periodically unstable glacier-fed slope, wherein the preserved facies associations and their stacking patterns are typical of ice-proximal subaqueous sediment complexes. Such complexes can accumulate within both freshwater and marine subaqueous settings, but the latter is favoured here due to the close stratigraphic association with thick carbonate successions both underlying and overlying the Kingston Peak Formation (Macdonald et al., 2013), and occurring as km-scale intraformational olistoliths in the neighbouring Kingston Range (Le Heron et al., 2014b). Moreover, the vast preserved sediment thicknesses, >600 m in this study

and >400 m in the Kingston Range (Le Heron et al., 2014b), far exceed recorded examples from glacilacustrine systems (e.g. Etienne et al., 2006; Johnsen & Brennand, 2004, 2006; Winsemann et al., 2007; Livingstone et al., 2010; Perkins & Brennand, in press).

The external geometry of the succession, i.e. whether it represents a radial (fan-shaped) or linear (apron) morphology, cannot be determined with certainty from the palaeocurrent data (**Fig. 1C**). It is recognised that a sufficiently expansive fan would also yield a very consistent palaeoflow (in this case to the SE) over a small portion of its surface, and therefore these patterns are not necessarily indicative of a linear input. Moreover, at contemporary ice sheet margins, ice streams frequently focus sediment distribution to specific points along the ice front (Stokes & Clark, 2001; Bennett, 2003; Ó'Cofaigh et al., 2003), restricting broad, linear sediment routing systems. The absence of correlative sections immediately along strike precludes investigation of the 3D architecture of this subaqueous system, and thus the control on sediment distribution patterns remains subject to further investigation. Nonetheless, the almost 100% continuity within the studied section affords great vertical resolution. The evolution of this subaqueous system will be described in five key stages below, as illustrated in **Fig. 8**. Each of these stages corresponds to ascending stratigraphic levels on the measured sections.

1. Ice distal outwash (0 - 116 m)

The base of the section is composed almost exclusively of the interbedded heterolithics facies association, where sandstone interbeds are typically thinner, finer grained and less frequent than further upsection, separated by thicker laminated siltstone units (**Fig. 2**). The stacked, coarsening upwards lobe elements are not preserved. Evidence of glacial influence on sedimentation is restricted to two thin intervals of lonestone-bearing siltstone. The first occurs towards the middle of this stage (70 m) and is accompanied by two thin beds of erosively based pebble conglomerate. The second example occurs towards the top of this stage (c. 112 m), and is truncated by a prominent erosion surface beneath a thicker cobble to pebble conglomerate. Isolated lonestones are interpreted to record iceberg rafting. Their close association with the infrequent conglomerate horizons is used to argue for contemporaneous pulses of sediment and iceberg distribution into the basin, possibly driven either by minor ice front oscillations, or as a product of debris destabilisation and remobilisation during calving processes at the terminus. The scarcity of these event beds, rare ice-rafting and overall fine grained nature of the sediments indicates an ice-distal/ice-medial setting on the margins of the subaqueous fan complex (**Fig. 8-1**).

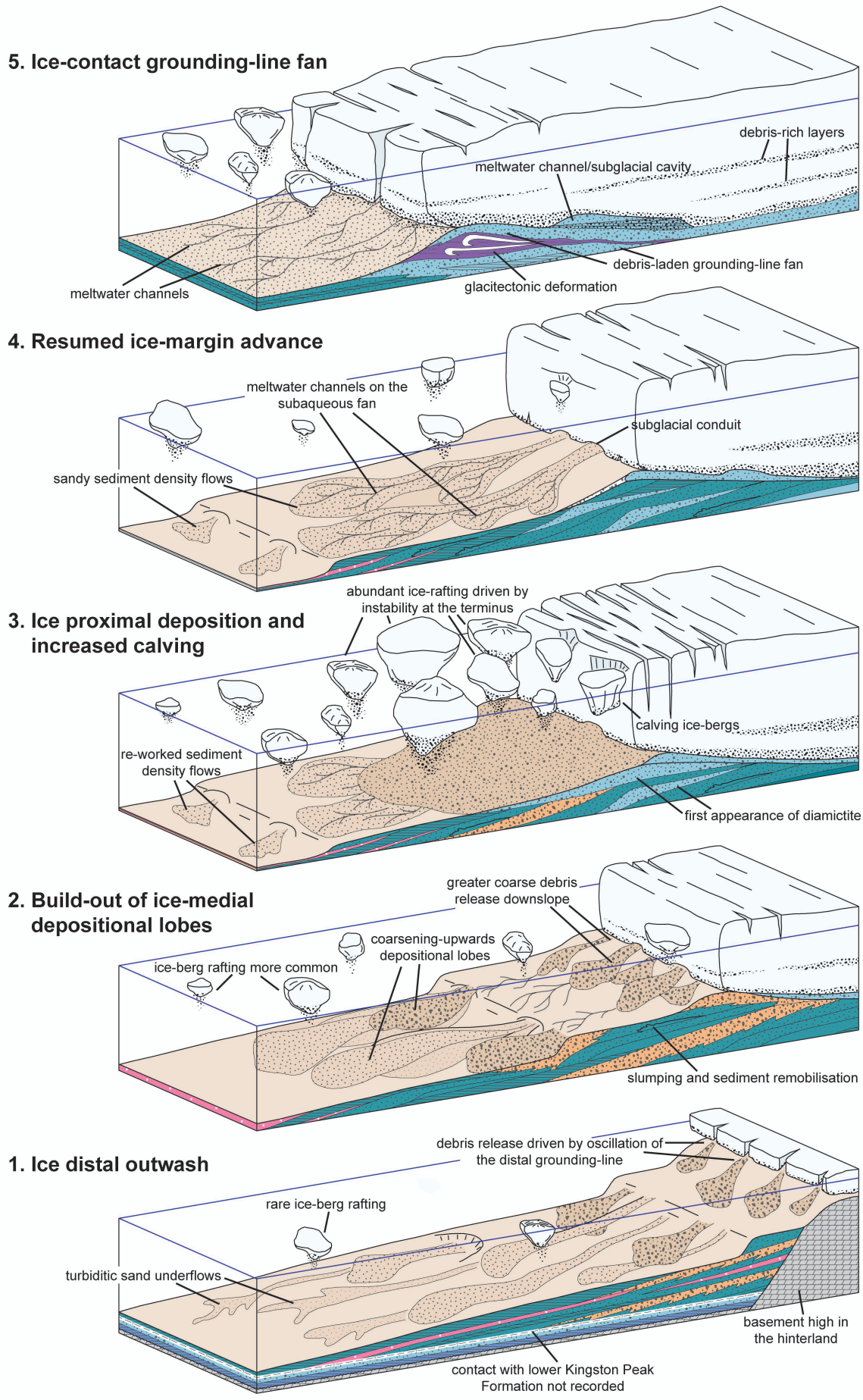

Fig. 8: Five stage depositional model demonstrating stepwise evolution of the glacier-fed subaqueous fan, see text for detailed description. Overall, a clear ice advance signature can be recognised, driving progradation of the subaqueous fan complex and an increase in glacial indicators up-section. This advance is subject to minor retreats and meltback phases, and thus supports dynamic ice sheet behaviour.

2. *Build-out of ice-medial depositional lobes (116 – 352 m)*

The development of an onlap surface onto the thick pebble to boulder conglomerate, discussed above, is interpreted to record local transgression, possibly driven by minor ice meltback in the hinterland. Above this horizon, turbidites are coarser and volumetrically much more abundant than below (interbedded heterolithics facies association), and frequently occur as stacked lobe elements (**Fig. 2**). The lonestone-bearing and pebble to boulder conglomerate facies associations occur at thicker and more regular intervals, the latter commonly representing the peak of lobe build-out. Direct evidence of glaciation is again restricted to ice-rafted debris, albeit with more abundant and larger lonestones than the distal outwash setting below.

The initiation, growth and abandonment of depositional lobes on the glacier-fed shelf is interpreted to be driven by pulsed sediment delivery downslope from the ice front (e.g. Laberg & Vorren, 1995, 2000; Vorren et al., 1998; Dimakis et al., 2000; Benn & Evans, 2010), possibly triggered by a periodically unstable or oscillating ice front (**Fig. 8-2**). This setting promotes abundant and regular, though not necessarily sustained, sediment supply, enabling lobe build-out during periods of elevated sediment remobilisation (grounding-line advance/oscillation), followed by lobe abandonment and increased hemipelagic sedimentation during periods of quiescence (grounding-line retreat).

3. *Ice proximal deposition and increased calving (352 – 476 m)*

The first appearance of diamictite (353 m, **Fig. 2**) records the onset of an ice proximal regime. In more distal settings, debrites (diamictite facies association) become more diluted, undergoing flow transformation to deposit turbidites of the interbedded heterolithics and pebble to boulder conglomerate facies associations. In the ice-proximal zone, co-genetic turbidites are significantly less abundant, whereas diamictic debrites occur repeatedly throughout the succession. The predominance of debrites over co-genetic turbidites suggests limited flow transformation, attributed to a shorter transport distance and therefore less opportunity for mixing and dilution. This is used to support proximity to the ice margin (**Fig. 8-3**), further corroborated by the more regular recurrence of ice-rafted debris, and the preservation of subglacially striated clasts.

Diamictite continuously more prevalent upsection, mirrored by an increase of IRD. Towards the top of this sequence a significant increase in calving processes at the ice front is recorded in a thick accumulation of iceberg rain-out diamictite (**Fig. 8-3**). This is considered to reflect increased instability at the ice front,

triggering more widespread calving and greater iceberg distribution basinward. These processes have the capacity to destabilise the ice margin (Benn et al., 2007 and references within), potentially halting ice advance temporarily, or initiating a retreat phase. The latter is favoured here due to the resumed dominance of turbidites, more akin to the depositional characteristics of Stage 2 described above.

4. *Resumed ice-margin advance (476 – 580 m)*

Above the iceberg rain-out deposit, the trend of more prevalent diamictite deposits upsection desists, replaced by renewed ice-medial turbidity currents of the interbedded heterolithics and pebble to boulder conglomerate facies associations. Initiation and growth of depositional lobes is again attributed to oscillation of the grounding-line, driving iceberg release and debris mass transport into the basin. At this stage, subglacial conduits feed meltwater channels on the glacier-fed shelf (e.g. Fleming, 2014), supporting more ice-proximal conditions (**Fig. 8-4**). This is accompanied by renewed accumulation of ice-proximal diamictites, which are now also channelised in places (543 m, **Fig. 2**), in contrast to lower in the sequence (Stage 3). These features in tandem with the greater preservation of ripple cross-lamination is suggestive of enhanced meltwater modification, consistent with increasing proximity of the glacier terminus. This also promotes elevated tractional re-working, leading to generation of the starved ripple and 'banded' facies described above. Channelisation in this portion of the subaqueous fan system is considered to contribute to debris bypass downslope, thereby depositing a greater accumulaton of inter-channel siltstones towards the top of this portion of the sequence (c. 544-580 m, **Fig. 2**).

5. *Growth of ice-contact grounding-line fan (580 – 636 m)*

At the top of the studied section a thick assemblage of glaciogenic debris flows (diamictite facies association) isinterpreted to accumulate within an ice-marginal grounding-line fan (**Fig. 8-5**). Ice-marginal fans typically build-up steep slopes (Powell, 1990; Lønne, 1995; Lønne & Nemec 2011a, , promoting sediment gravity flow remobilisation downslope on both the ice-proximal and ice-distal fan margins. This process is thought to account for the preservation of slump folds verging perpendicular to the principal palaeoflow orientation recorded throughout the remainder of the succession (**Fig. 1C**). In line with similar studies of ice-marginal subaqueous fan systems, impact-related deformation structures are not recognised (L nne, 1995), although ice-rafting processes remain an important source of coarse debris.

Locally, the glacier terminus is considered to advance to an ice-contact position, leading to proglacial glacitectonic thrusting of the finer grained, and therefore less competent facies (tectonised facies association). The dominantly ductile style of deformation supports elevated porewater pressures, attributed to a combination of dilute, water-rich sediment flows, the input of abundant meltwater and potentially overburden pressure of the advancing ice margin. The glacitectonic thrusting and high sediment supply may also contribute to thrust-stacking and thickening of the ice-marginal sediment pile. Onlap surfaces towards the top of the succession (at 628 and 634 m, **Fig. 2**) are interpreted to record local flooding of the grounding-line fan, driven by stillstand or early retreat of the ice front. At this stage, hemipelagic and sediment density flow sediments return. However, truncation of the top of the succession beneath the Noonday Dolomite obscures the full extent of retreat.

ICE SHEET DYNAMICS

Overall, a clear ice advance signature can be recognised within the Sperry Wash succession, where ice distal environments are succeeded by medial, proximal and finally ice-marginal to ice-contact depositional settings. An advance sequence is recorded throughout the ice distal outwash (Stage 1), advancing through ice-medial settings (Stage 2) to an ice-proximal position (Stage 3). Throughout this sequence the ice margin is considered to become increasingly unstable, driving more widespread calving and increasingly greater iceberg distribution into the basin. This instability triggers a minor retreat phase, leading to resumed ice-medial conditions and a subsequent re-advance through ice-proximal (Stage 4) and finally ice-marginal settings (Stage 5), with evidence of local advance to an ice-contact position. Thus, basinward progradation of the subaqueous fan progresses throughout, subject to minor back-stepping, and is driven by dominant advance and minor retreat of the ice front (**Fig. 8**).

Regional mapping places the Sperry Wash sections in unit KP3 (e.g. Prave, 1999; Mrofka & Kennedy, 2011), permitting detailed comparison with other Death Valley outcrop belts. In the type area of the Kingston Range, unit KP3 is punctuated by an olistostrome succession at least 1.5 km in thickness (Macdonald et al., 2013; Le Heron et al., 2014b).
sequence has been interpreted as recording a significant ice meltback event, corresponding to glacial minimum conditions during the Sturtian glaciation (Le Heron et al., 2014b). Following this event, widespread re-advance of the ice front is recorded in both the northern and southern Kingston Range (Le Heron et al., 2014b; Le Heron & Busfield, this volume), depositing a succession of proglacial turbidites and glaciogenic debris flows

(GDFs). In the northern sections boulder conglomerates and coarse sandstones dominate, whereas further south fine-grained siltstones and sandstones are notably abundant, interpreted to reflect proximal to distal facies trends.

The siltstone and sandstone dominated deposits of the southern Kingston Range compare closely to the Sperry Wash study interval, although thicker bedded conglomeratic intervals are more comparable to the northern Kingston Range sections (Le Heron et al., 2014b; Le Heron & Busfield, this volume). Regular and stacked diamictite deposits within unit KP3, however, appear to be unique to the Sperry Wash succession. This represents an important distinction in the progress of ice advance across the three study intervals. In the Kingston Range, following the glacial minimum, ice sheets re-advanced to deposit ice-proximal sediments, within an exclusively proglacial position. At Sperry Wash, ice advance continues from ice-distal settings comparable to the southern Kingston Range (Le Heron & Busfield, this volume), through ice-proximal settings of the northern Kingston Range, to ice-marginal depositional environments. The top of each succession is truncated beneath the Noonday Dolomite, and therefore this disparity may simply reflect differential preservation. Alternatively, this change may be driven by basin configuration. Under this scenario, two configurations are plausible, although neither are mutually exclusive: 1) the northern and southern Kingston Range represent deeper and more distal 'slope' settings and Sperry Wash the shallower and more proximal 'shelf' (see Le Heron & Busfield, this volume), or 2) the Sperry Wash succession was deposited in a narrower basin, leading to a more pronounced progradation signature. These tentative scenarios require further testing by comparison to other outcrop belts.

CONCLUSIONS

The Sperry Wash succession allows detailed insight into the dynamics of Sturtian ice sheets as recorded in a marine succession dominated by gravity flows. The succession belongs to the upper part of the Kingston Peak Formation in a stratigraphic unit previously defined as unit KP3 (Prave, 1999; Macdonald et al., 2013). Sedimentological analysis of a 636 m measured section demonstrates that a clear, overall ice sheet advance signature can be recognised. Unique to this section, by comparison to other Death Valley outcrop belts, are ice-marginal and ice-contactdeposits which are identifiable by a characteristic deformation zone near the top of the studied section. These features allow us to posit that grounding line zones can be established in Neoproterozoic successions, with great capacity for mapping out the as yet unknown true scale of these 'pan-global' ice masses. Moreover,

the style and influence of advance-retreat cycles is demonstrated to vary considerably over neighbouring outcrop belts, allowing an insight into the complexity of Sturtian glaciodynamics within only a small region of its arguably global extent.

ACKNOWLEDGEMENT

Field data collection was supported by the Fermor Fund of the Geological Society of London.

REFERENCES

Allen, J.R.L. 1982. *Sedimentary Structures, Their Character and Physical Basis*. Elsevier, Amsterdam, 395-431.

Allen, J.R.L. 1991. The Bouma A division and the possible duration of turbidity currents. *Journal of Sedimentary Petrology*, **61**, 291-295.

Allen, P.A., Leather, J. & Brasier, M.D. 2004. The Neoproterozoic Fiq glaciation and its aftermath, Huqf supergroup of Oman. *Basin Research*, **16**, 507-534.

Arnaud, E. 2012. The paleoclimatic significance of deformation structures in Neoproterozoic successions. *Sedimentary Geology*, **243-244**, 33–56.

Baas, J.H. 2000. Duration of deposition from decelerating high-density turbidity currents. *Sedimentary Geology*, **136**, 71-88.

Baas, J.H., Best, J.L. & Peakall, J. 2011. Depositional processes, bedform development and hybrid flows in rapidly decelerated cohesive (mud-sand) sediment flows. *Sedimentology*, **58**, 1953-1987.

Benn, D. I., Warren, C. R., & Mottram, R. H. 2007. Calving processes and the dynamics of calving glaciers. *Earth-Science Reviews*, **82**, 143-179.

Benn, D.I. & Evans, D.J.A. 2010. *Glaciers and Glaciation*. Hodder Education, London, 802 p.

Bennett, M.R. 2003. Ice streams as the arteries of an ice sheet: their mechanics, stability and significance. *Earth-Science Reviews*, **61**, 309–339.

Bowring, S.A., Grotzinger, J.P., Condon, D.J., Ramezani, J. & Newall, M. 2007. Geochronologic constraints on the chronostratigraphic framework of the Neoproterozoic Huqf Supergroup, Sultanate of Oman. *American Journal of Science*, **307**, 1097-1145.

Boulton, G. S. 1978. Boulder shapes and grain-size distributions of debris as indicators of transport paths through a glacier and till genesis. *Sedimentology*, **25**, 773-799.

Busfield, M. E., & Le Heron, D. P. 2013. Glacitectonic deformation in the Chuos Formation of northern Namibia: implications for Neoproterozoic ice dynamics. *Proceedings of the Geologists' Association*, **124**, 778–789.

Busfield, M. E., & Le Heron, D. P. 2014. Sequencing the Sturtian icehouse: dynamic ice behaviour in South Australia. *Journal of the Geological Society, London*, **171**, 443-456.

Condon, D.J., Zhu, M., Bowring, S.A., Wang, W., Yang, A. & Jin, Y. 2005. U-Pb ages from the Neoproterozoic Doushantuo Formation, China. *Science*, **308**, 95-98.

Denis, M., Guiraud, M., Konaté, M., Buoncristiani, J.F., 2010. Subglacial deformation and water-pressure cycles as a key for understanding ice stream dynamics: evidence from the Late Ordovician succession of the Djado Basin (Niger).

International Journal of Earth *Sciences*, **99**, 1399-1425.

Dimakis, P., Elverhøi, A., Høeg, K., Solheim, A., Harbitz, C., Laberg, J. S. & Marr, J. 2000. Submarine slope stability on high-latitude glaciated Svalbard–Barents Sea margin. *Marine Geology*, **162**, 303-316.

Dowdeswell, J. A. 1986. The distribution and character of sediments in a tidewater glacier, southern Baffin Island, NWT, Canada. *Arctic and Alpine Research*, **18**, 45-56.

Dowdeswell, J. A. 1989. On the nature of Svalbard icebergs. *Journal of Glaciology*, **35**, 224-234.

Elverhøi, A., de Blasio, F. V., Butt, F. A., Issler, D., Harbitz, C., Engvik, L. & Marr, J. 2002. Submarine mass-wasting on glacially-influenced continental slopes: processes and dynamics. *The Geological Society, London, Special Publication*, **203**, 73-87.

Etienne, J.L., Jansson, K.N., Glasser, N.F., Hambrey, M.J., Davies, J.R., Waters, R.A., Maltman, A.J. & Wilby, P.R. 2006. Palaeoenvironmental interpretation of an ice-contact glacial lake succession: an example from the late Devensian of southwest Wales, UK. *Quaternary Science Reviews*, **25**, 739-762.

Evans, D.J.A. & Hiemstra, J.F. 2005. Till deposition by glacier submarginal, incremental thickening. *Earth Surface Processes and Landforms*, **30**, 1633–1662.

Evans, D.J.A., Hiemstra, J.F. & Ó'Cofaigh, C. 2012. Stratigraphic architecture and sedimentology of a Late Pleistocene subaqueous moraine complex, southwest Ireland. *Journal of Quaternary Science*, **27**, 51–63.

Evans, J., & Pudsey, C. J. 2002. Sedimentation associated with Antarctic Peninsula ice shelves: implications for palaeoenvironmental reconstructions of glacimarine sediments. *Journal of the Geological Society, London*, **159**, 233-237.

Fairchild, I.J. & Kennedy, M.J. 2007. Neoproterozoic glaciation in the Earth System. *Journal of the Geological Society, London*, **164**, 895-921.

Fleming, E.J. 2014. *Magnetic, structural and sedimentological analysis of glacial sediments: insights from modern, Quaternary and Neoproterozoic environments.* PhD thesis, University of Birmingham, UK, 354 p.

Hammond, J.G. 1983. *Late Precambrian diabase intrusions in the southern Death Valley region, California: their petrology, geochemistry, and tectonic implications.* PhD thesis, University of Southern California, 281 p.

Hampton, M.A. 1972. The role of subaqueous debris flow in generating turbidity currents. *Journal of Sedimentary Petrology*, **42**, 775-793.

Hazzard, J.C. 1937. Paleozoic section in the Nopah and Resting Springs Mountains, Inyo County, California. *California Journal of Mines and Geology*, **33**, 270-339.

Heaman, L.M. & Grotzinger, J.P. 1992. 1.08 Ga diabase sills in the Pahrump Group, California; implications for development of the Cordilleran miogeocline. *Geology*, **20**, 637-640.

Henry, L.C., Isbell, J.F., Fielding, C.R., Domack, E.W., Frank, T.D. & Fraiser, M.L. 2012. Proglacial deposition and deformation in the Upper Carboniferous to Lower Permian Wynyard Formation, Tasmania: a process analysis. *Palaeogeography, Palaeoclimatology, Palaeoecology*, **315-316**, 142-157.

Hewett, D.F. 1940. New formation names to be used in the Kinsgton Range, Ivanpah Quadrangle, California. *Journal of the*

Washington Academy of Sciences, **30**, 239-240.

Hewett, D.F. 1956. Geology and Mineral Resources of the Ivanpah Quadrangle, California and Nevada. *US Geological Survey Professional Paper 275*, 172 p.

Hiemstra, J.F. & Rijsdijk, K.F., 2003. Observing artificially induced strain: implications for subglacial deformation. *Journal of Quaternary Science*, **18**, 373-383.

Hiemstra, J.F. & van der Meer, J.J.M., 1997. Pore-water controlled grain fracturing as an indicator for subglacial shearing in tills. *Journal of Glaciology*, **43**, 446-454.

Hodgson, D.M., Flint, S.S., Hidgetts, D., Drinkwater, N.J., Johannessen, E.P. & Luthi, S. 2006. Stratigraphic evolution of fine-grained submarine fan systems, Tanqua depocentre, Karoo Basin, South Africa. *Journal of Sedimentary Research*, **76**, 20-40.

Hoffman, P. F. 1998. A Neoproterozoic Snowball Earth. *Science*, **281**, 1342–1346.

Hoffman, P.F. 2009. Pan-glacial – a third state in the climate system. *Geology Today*, **25**, 100-107.

Hoffmann, K.-H., Condon, D. J., Bowring, S. a., & Crowley, J. L. 2004. U-Pb zircon date from the Neoproterozoic Ghaub Formation, Namibia: Constraints on Marinoan glaciation. *Geology*, **32**, 817-820.

Ilstad, T., Elverhøi, A., Issler, D., & Marr, J. G. 2004. Subaqueous debris flow behaviour and its dependence on the sand/clay ratio: a laboratory study using particle tracking. *Marine Geology*, **213**, 415-438.

Jennings, C.W., Burnett, J.L. & Troxel, B.W. 1962. Geologic Map of California – Trona Sheet. Division of Mines and Geology, California.

Jobe, Z.R., Lowe, D.R. & Morris, W.R. 2012. Climbing-ripple successions in turbidite systems: depositional environments, sedimentation rates and accumulation times. *Sedimentology*, **59**, 867-898.

Johnsen, T.F. & Brennand, T.A. 2004. Late glacial lakes in the Thompson basin, British Columbia: palaeogeography and evolution. *Canadian Journal of Earth Sciences*, **41**, 1367-1383.

Johnsen, T.F. & Brennand, T.A. 2006. The environment in and around ice-dammed lakes in the moderately high relief setting of the southern Canadian Cordillera. *Boreas*, **35**, 106-125.

Kane, I.A. & Hodgson, D. 2010. Submarine channel levees, criteria for recognition of subenvironments: exhumed examples from the Rosario Fm (Baja, Mexico) and the Laingsburg Fm (Karoo Basin). *Marine and Petroleum Geology*, **28**, 807-823.

Kneller, B. 1995. Beyond the turbidite paradigm: physical models for deposition of turbidites and their implications for reservoir prediction. *The Geological Society, London, Special Publication,* **94**, 31-31.

Komar, P.D. 1985. The hydraulic interpretation of turbidites from their grain sizes and sedimentary structures. *Sedimentology*, **32**, 395-407.

Kuenen, P.H. 1966. Experimental turbidite lamination in a circular flume. The Journal of *Geology*, **74**, 523-545.

Kuenen, P.H. & Humbert, F.L. 1969. Grain size of turbidite ripples. *Sedimentology*, **13**, 253-261.

Laberg, J.S., & Vorren, T. O. 1995. Late Weichselian submarine debris flow deposits on the Bear Island Trough mouth fan. *Marine Geology*, **127**, 45-72.

Laberg, J.S., & Vorren, T. O. 2000. Flow behaviour of the submarine glacigenic debris flows on the Bear Island Trough Mouth Fan, western Barents Sea. *Sedimentology*, **47**, 1105-1117.

Labotka, T.C., Albee, A.L., Lanphere, M.A. & McDowell, S.C. 1980. Stratigraphy, structure and metamorphism in the central Panamint Mountains (Telescope Peak quadrangle), Death Valley area, California. *Geological Society of America Bulletin*, **91**, 843-933.

Lachniet, M.S., Larson, G.J., Lawson, D.E., Evenson, E.B., Alley, R.B., 2001. Microstructures of sediment flow deposits and subglacial sediments: a comparison. *Boreas*, **30**, 254-264.

Le Heron, D.P. & Busfield, M.E. this volume. Pulsed iceberg delivery driven by Sturtian ice sheet dynamics: an example from Death Valley, California. *Sedimentology*.

Le Heron, D. P., Cox, G., Trundley, a., & Collins, A. 2011. Sea ice-free conditions during the Sturtian glaciation (early Cryogenian), South Australia. *Geology*, **39**, 31–34.

Le Heron, D. P., Busfield, M. E., & Kamona, F. 2013. An interglacial on snowball Earth? Dynamic ice behaviour revealed in the Chuos Formation, Namibia. *Sedimentology*, **60**, 411–427.

Le Heron, D. P., Busfield, M. E., & Collins, A. S. 2014a. Bolla Bollana boulder beds: A Neoproterozoic trough mouth fan in South Australia? *Sedimentology*, **61**, 978-995.

Le Heron, D.P., Busfield, M.E. & Prave, A.R. 2014b. Neoproterozoic ice sheets and olistoliths: multiple glacial cycles in the Kingston Peak Formation, California. *Journal of the Geological Society, London*, **171**, 525-538.

Leclair, S. F., & Arnott, R. W. C. 2005. Parallel lamination formed by high-density turbidity currents. *Journal of Sedimentary Research*, **75**, 1-5.

Lee, J.R. & Phillips, E.R., 2008. Progressive soft sediment deformation within a subglacial shear zone—a hybrid mosaic–pervasive deformation model for Middle Pleistocene glaciotectonised sediments from eastern England. *Quaternary Science Reviews*, **27**, 1350-1362.

Livingstone, S.J., Ó'Cofaigh, C. & Evans, D.J.A. 2010. A major ice drainage pathway of the last British-Irish Ice Sheet: the Tyne Gap, northern England. *Journal of Quaternary Science*, **25**, 354–370.

Lønne, I. 1995. Sedimentary facies and depositional architecture of ice-contact glaciomarine systems. *Sedimentary Geology*, **98**, 13-43.

Lønne, I., & Nemec, W. 2011a. Modes of sediment delivery to the grounding line of a fast-flowing tidewater glacier: implications for ice-margin conditions and glacier dynamics. *The Geological Society, London, Special Publication*, **354**, 33–56.

Lønne, I., & Nemec, W. 2011b. The kinematics of ancient tidewater ice margins: criteria for recognition from grounding-line moraines. *The Geological Society, London, Special Publication*, **354**, 57–75.

Lowe, D. R. 1982. Sediment gravity flows: II Depositional models with special reference to the deposits of high-density turbidity currents. *Journal of Sedimentary Research*, **52**, 279-

Lowe, D. R. 1988. Suspended-load fallout rate as an independent variable in the analysis of current structures. *Sedimentology*, **35**, 765-776.

Macdonald, F.A., Schmitz, M.D., Crowley, J.L., Roots, C.F., Jones, D.S., Maloof, A.C., Strauss, J.V., Cohen, P.A., Johnston, D.T. & Schrag, D.P. 2010. Calibrating the Cryogenian. *Science*, **327**, 1241-1243.

Macdonald, F. A., Prave, A. R., Petterson, R., Smith, E. F., Pruss, S. B., Oates, K., Fallick, A. E. 2013. The Laurentian record of Neoproterozoic glaciation, tectonism, and eukaryotic evolution in Death Valley, California. *Geological Society of America Bulletin*, **125**, 1203–1223.

Macdonald, H. A., Peakall, J., Wignall, P. B., & Best, J. 2011. Sedimentation in deep-sea lobe-elements: implications for the origin of thickening-upward sequences. *Journal of the Geological Society*, **168**, 319–332.

Mahon, R. C., Dehler, C. M., Link, P. K., Karlstrom, K. E., & Gehrels, G. E. 2014. Geochronologic and stratigraphic constraints on the Mesoproterozoic and Neoproterozoic Pahrump Group, Death Valley, California: A record of the assembly, stability, and breakup of Rodinia. *Geological Society of America Bulletin*, **126**, 652-664.

Maltman, A. 1994. *The Geological Deformation of Sediments*. Chapman and Hall, Cambridge, 384 p.

Marenssi, S.A., Tripaldi, A., Limarino, C.O. & Caselli, A.T. 2005. Facies and architecture of a Carboniferous grounding-line system from the Guandacol Formation, Paganzo Basin, northwestern Argentina. *Gondwana Research*, **8**, 187-202.

Menzies, J. 2000. Micromorpholigcal analyses of microfabrics and microstructures indicative of deformation processes in glacial sediments. In: Maltman, A.J., Hubbard, B., Hambrey, M.J. (eds.) *Deformation of Glacial Materials*. Geological Society Special Publication No. 176, London, p. 245-257.

Menzies, J. & Zaniewski, K., 2003. Microstructures within a modern debris flow deposit derived from Quaternary glacial diamicton—a comparative micromorphological study. *Sedimentary Geology*, **157**, 31-48.

Middleton, G.V. & Hampton, M.A. 1973. Sediment gravity flows: mechanisms of flow and deposition. In: Middleton, G.V. & Bouma, A.H. (eds.) *Turbidites and Deep-water Sedimentation*. SEPM Pacific Section, Short Course Lecture Notes, 1-38.

Miller, J.M.G. 1985. Glacial and syntectonic sedimentation: the Upper Proterozoic Kingston Peak Formation, southern Panamint Range, eastern California. *Geological Society of America Bulletin*, **96**, 1537-1553.

Mrofka, D. & Kennedy, M. 2011. The Kingston Peak Formation in the eastern Death Valley region. In: Arnaud, E., Halverson, G. & Shields-Zhou, G. (eds.) *The Geological Record of Neoproterozoic Glaciations*. Geological Society, London, Memoirs, **36**, 449-458.

Mulder, T. & Alexander, A. 2001. The physical character of subaqueous sedimentary density flows and their deposits. *Sedimentology*, **48**, 269-299.

Noble, L.F. 1934. Rock formations of Death Valley, CA. *Science*, **80**, 173-178.

Ó Cofaigh, C., Taylor, J., Dowdeswell, J.A., Rosell-Melé, A., Kenyon, N.H., Evans, J., & Mienert, J. 2002. Sediment reworking on high-latitude continental margins and its implications for palaeoceanographic studies: insights from the Norwegian-Greenland Sea. *The Geological Society, London, Special Publication*, **203**, 325-348.

Ó'Cofaigh, C., Taylor, J., Dowdeswell, J.A. & Pudsey, C.J. 2003. Palaeo-ice streams, trough mouth fans and high-latitude continental slope sedimentation. *Boreas*, **32**, 37-55.

Ó'Cofaigh, C., Evans, D.J.A. & Hiemstra, J.F. 2011. Formation of a stratified subglacial 'till' assemblage by ice-marginal thrusting and glacier overriding. *Boreas*, **40**, 1-14.

Ovenshine, A. T. 1970. Observations of iceberg rafting in Glacier Bay, Alaska, and the

identification of ancient ice-rafted deposits. *Geological Society of America Bulletin*, **81**, 891-894.

Perkins, A.J. & Brennand, T.A. *in press*. Refining the pattern and style of Cordilleran Ice Sheet retreat: palaeogeography, evolution and implications of lateglacial ice-dammed lake systems on the southern Fraser Plateau, British Columbia, Canada. *Boreas*, doi: 10.1111/bor.12100.

Petterson, R., Prave, A.R., Wernicke, B.P. & Fallick, A.E. 2011a. The Neoproterozoic Noonday Formation, Death Valley region, California. *Geological Society of America Bulletin*, **123**, 1317-1336.

Petterson, R., Prave, a. R., & Wernicke, B. P. 2011b. Glaciogenic and related strata of the Neoproterozoic Kingston Peak Formation in the Panamint Range, Death Valley region, California. *In:* Arnaud, E., Halverson, G.P. & Shields-Zhou, G. (eds.) *The Geological Record of Neoproterozoic Glaciations*. Geological Society, London, Memoirs, **36**, 449-458.

Phillips, E., 2006. Micromorphology of a debris flow deposit: evidence of basal shearing, hydrofracturing, liquefaction and rotational deformation during emplacement. *Quaternary Science Reviews*, **25**, 720-738.

Phillips, E., Merritt, J., Auton, C., Golledge, N., 2007. Microstructures in subglacial and proglacial sediments: understanding faults, folds and fabrics, and the influence of water on the style of deformation. *Quaternary Science Reviews*, **26**, 1499-1528.

Piper, D.J.W 1978. Turbidite muds and silts on deep sea fans and abyssal plains. In: Stanley, D.J. & Kelling, G. (eds.) *Sedimentation in Submarine Canyons, Fans and Trenches*. Hutchinson and Ross, Pennsylvania, 163-176.

Postma, G., Nemec, W., Kleinspehn, K.L., 1988. Large Floating Clasts in Turbidites - a Mechanism for Their Emplacement. *Sedimentary Geology*, **58**, 47-61.

Powell, R.D. 1990. Glacimarine processes at grounding-line fans and their growth into ice-contact deltas. In: Dowdeswell, J.A. & Scourse, J.D. (eds.) *Glacimarine Environments: Processes and Sediments*. The Geological Society, London, Special Publication, 53, 53-73.

Powell, R.D. & Domack, E.W. 2002. Modern glacimarine environments. In: Menzies, J. (ed.) *Modern and Past Glacial Environments*. Butterworth-Heinemann Ltd., Oxford, 361-389.

Prave, A.R. 1999. Two diamictites, two cap carbonates, two $\delta^{13}C$ excursions, two rifts: the Neoproterozoic Kingston Peak Formation, Death Valley, California. *Geology*, **27**, 339-342.

Prélat, A., & Hodgson, D. M. 2013. The full range of turbidite bed thickness patterns in submarine lobes: controls and implications. *Journal of the Geological Society*, **170**, 209-214.

Prélat, A., Hodgson, D. M., & Flint, S. 2009. Evolution, architecture and hierarchy of distributary deep-water deposits: a high-resolution outcrop investigation from the Permian Karoo Basin, South Africa. *Sedimentology*, **56**, 2132-2154.

Ravier, E., Buoncristiani, J.-F., Clerc, S., Guiraud, M., Menzies, J., & Portier, E. (2014). Sedimentological and deformational criteria for discriminating subglaciofluvial deposits from subaqueous ice-contact fan deposits: A Pleistocene example (Ireland). *Sedimentology*, doi:10.1111/sed.12111

Stokes, C.R. & Clark, C.D. 2001. Palaeo-ice streams. *Quaternary Science Reviews*, **20,** 1437-1457.

Sumner, E. J., Amy, L. A., & Talling, P. J. 2008. Deposit structure and processes of sand

deposition from decelerating sediment suspensions. *Journal of Sedimentary Research*, **78**, 529-547.

Sylvester, Z. & Lowe, D.R. 2004. Textural trends in turbidites and slurry beds from the Oligocene flysch of the Carpathians, Romania. *Sedimentology*, **51**, 945-972.

Talling, P.J., Amy, L.A., Wynn, R.B., Blackbourn, G. & Gibson, O. 2007. Turbidity current evolution deduced from extensive thin turbidites: Marnosos-arenacea Formation (Miocene), Italian Appenines. *Journal of Sedimentary Research*, **77**, 172-196.

Talling, P. J., Masson, D. G., Sumner, E. J., & Malgesini, G. 2012. Subaqueous sediment density flows: Depositional processes and deposit types. *Sedimentology*, **59**, 1937–2003.

Talling, P. J. 2013. Hybrid submarine flows comprising turbidity current and cohesive debris flow: Deposits, theoretical and experimental analyses, and generalized models. *Geosphere*, **9**, 460-488.

Troxel, B.W. 1966. Sedimentary features of the later Precambrian Kingston Peak Formation, Death Valley, California. *Geological Society of America Special Paper 101*, 341 p.

Troxel, B.W. 1982. Description of the uppermost part of the Kingston Peak Formation, Amargosa Rim Canyon, Death Valley region, California. In: Cooper, J.D., Troxel, B.W. & Wright, L.A. (eds.) *Geology of selected areas in the San Bernardino Mountains, western Mojave Desert, and southern Great Basin, California.* Geological Society of America Cordilleran Section Field Trip Guidebook and Volume. Death Valley Publishing Company, Shoshone, California, p. 61-70.

Vorren, T. O., Laberg, J. S., Blaume, F., Dowdeswell, J. A., Kenyon, N. H., Mienert, J. & Werner, F. 1998. The Norwegian–Greenland Sea continental margins: morphology and late Quaternary sedimentary processes and environment. *Quaternary Science Reviews*, **17**, 273-302.

Walker, R.G. 1967. Turbidite sedimentary structures and their relationship to proximal and distal depositional environments. *Journal of Sedimentary Petrology*, **37**, 25-43.

Walker, R.G. 1978. Deep-water sandstone facies and ancient submarine fans – models for exploration and for stratigraphic traps. *AAPG Bulletin*, **62**, 932-966.

Winsemann, J., Asprion, U., Meyer, T., & Schramm, C. 2007. Facies characteristics of Middle Pleistocene (Saalian) ice-margin subaqueous fan and delta deposits, glacial Lake Leine, NW Germany. *Sedimentary Geology*, **193**, 105-129.

Wright, L.A. 1974. Geology of the Southeast Quarter of Tecopa Quadrangle, Inyo County, California. Californian Division of Mines and Geology Map Sheet.

Zaniewski, K. & van der Meer, J.J.M. 2005. Quantification of plasmic fabric through image analysis. *Catena*, **63**, 109-127.

Zhou, C., Tucker, R., Xiao, S., Peng, Z., Yuan, X. & Chen, Z. 2004. New constraints on the ages of Neoproterozoic glaciations in South China. *Geology*, **32**, 437-440.